Insufficient mass spectrometric detection of synthesized peroxy acids from α-pinene ozonolysis

Markus Tischberger[1], Rulan Verma[1], Johanna Breinsperger[2], David Schachamayr[2], Marco Lair[1], Melanie Opacak[1], Peter Gärtner[2], Hinrich Grothe[1], Maximilian Kaiser[2], and Dominik Stolzenburg[1]

[1]Institute of Materials Chemistry, TU Wien, Getreidemarkt 9, 1060 Vienna, Austria
[2]Institute of Applied Synthetic Chemistry, TU Wien, Getreidemarkt 9, 1060 Vienna, Austria

Correspondence: Maximilian Kaiser (maximilian.kaiser@tuwien.ac.at) and Dominik Stolzenburg (dominik.stolzenburg@tuwien.ac.at)

Abstract. Biogenic volatile organic compounds (BVOCs) are major precursors of secondary organic aerosol (SOA) and new particle formation (NPF), and therefore play an important role in the climate system, altering the abundance of cloud condensation nuclei (CCN). Ozonolysis of the most atmospherically abundant monoterpene, α-pinene, generates RO_2 radicals which undergo autoxidation, resulting in the formation of oxygenated organic molecules (OOMs) with low volatility, an essential step in nucleation and early particle growth. However, quantitative interpretation of widely used mass spectrometric OOM measurements remains limited by reagent-ion selectivity and the lack of authentic monomeric standards, an issue that is particularly important for hydroperoxides and peroxy acids, which constitute a significant fraction of autoxidation products. Here, we synthesize two α-pinene-derived monomeric OOM standards, peroxy norpinonic acid (PNPA; $C_9H_{14}O_4$) and peroxy pinonic acid (PPA; $C_{10}H_{16}O_4$), and confirm their structures by ^{1}H and ^{13}C NMR. We then evaluate their detectability using a MION-Orbitrap operated with nitrate (NO_3^-) and uronium ($CH_5N_2O^+$) chemical ionization and compare these gas-phase schemes to heated electrospray ionization (H-ESI). NMR shows that freshly prepared standards are dominated by peroxy acids and contain only a fraction of the corresponding carboxylic acids, whereas Orbitrap measurements consistently yield substantially lower peroxy-to-carboxylic-acid ratios. These ratios vary strongly across ionization modes, with greater apparent peroxy acid loss under harder (de)protonation and improved, though still incomplete, preservation under softer nitrate and uronium adduct formation. Together with the paired temporal profiles of the peroxy and carboxylic acid signals, the results are consistent with ionization-associated loss of peroxy acid functionality. Notably, uronium provides significantly higher sensitivity for these moderately oxygenated compounds, complementing nitrate's strong selectivity toward highly oxygenated organic molecules (HOMs). Together, our results suggest that peroxy acids formed via α-pinene autoxidation may be systematically under-quantified by commonly used mass spectrometric approaches, with possible implications for molecular assignments, oxygen-to-carbon (O:C) ratios, volatility-basis-set derivations, and inferred rates of nucleation and early particle growth. The broader atmospheric magnitude of these effects remains to be established.

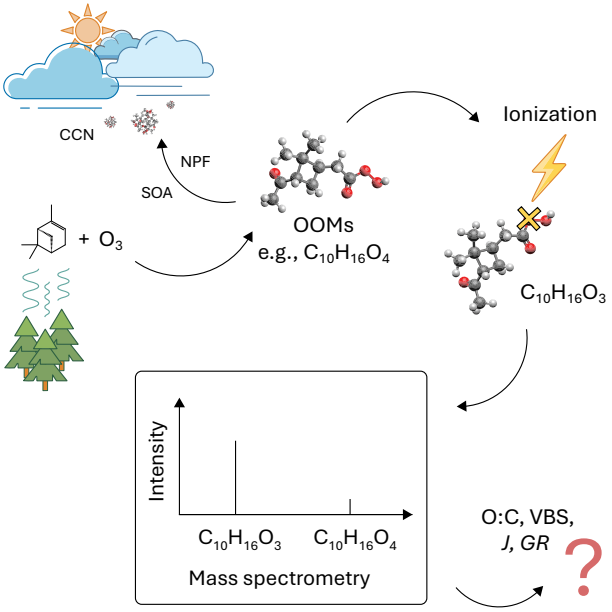

1 Introduction

Biogenic volatile organic compounds (BVOCs) are key precursors of secondary organic aerosol (SOA) (Hodzic et al., 2016), a major component of atmospheric particulate matter (Zhang et al., 2007; Hallquist et al., 2009; Jimenez et al., 2009) with profound implications for climate (IPCC, 2021) and human health (HEI, 2025; IHME, 2025). New particle formation (NPF), where molecules form thermodynamically stable clusters through nucleation and continue to grow to larger sizes (Kulmala, 2003), is the dominant source in terms of aerosol particle number concentration across most of the troposphere (Yu and Luo, 2009; Gordon et al., 2017) and contributes significantly to the particle and cloud condensation nuclei (CCN) budget in the continental boundary layer (Reddington et al., 2011; Fountoukis et al., 2012; Matsui et al., 2013; Lupascu et al., 2015; Posner and Pandis, 2015; Cai et al., 2016). Monoterpenes and particularly α-pinene ($C_{10}H_{16}$) emitted by trees contribute significantly to global BVOC emissions (Sindelarova et al., 2022) and have therefore become central to studies of SOA and NPF.

Upon reaction with atmospheric ozone, α-pinene ozonolysis is initiated, leading to the formation of peroxy radicals (RO_2) (Ehn et al., 2014; Kurtén et al., 2015) which can undergo autoxidation. In this process, consecutive intramolecular H-shifts followed by rapid O_2 additions produce increasingly oxygenated organic molecules (OOMs), often containing hydroperoxide [–OOH] or peroxy acid [–(C=O)OOH] functionalities. Their volatility can decrease to the regime of (extremely) low volatility organic compounds ((E)LVOC), enabling condensation onto existing molecular clusters or sufficiently large particles, or even direct participation in nucleation driven solely by ELVOC interactions in the case of highly oxygenated organic molecules (HOMs) (Ehn et al., 2014; Kirkby et al., 2016; Tröstl et al., 2016; Bianchi et al., 2019).

OOMs govern key stages of continental boundary layer NPF: covalently bound dimers serve as the main nucleators driving

cluster formation (Kirkby et al., 2016; Elm et al., 2017; Bianchi et al., 2019), while OOM monomers drive early particle growth due to their higher concentrations and low saturation vapor pressures (Tröstl et al., 2016; Qi et al., 2018; Stolzenburg et al., 2018).

The primary technique for measuring OOMs is chemical ionization (CI) mass spectrometry using nitrate (NO_3^-) as reagent ion, with the CI-APi-TOF being an especially prominent instrument (Bianchi et al., 2019). However, nitrate chemical ionization mass spectrometers (CIMS) are less sensitive towards less oxygenated analytes (Riva et al., 2019b), which are still decisive for particle growth, especially at lower temperatures (Stolzenburg et al., 2018). Orbitrap mass spectrometry coupled with the multischeme chemical ionization inlet (MION) is an emerging and promising technique (Rissanen et al., 2019; Riva et al., 2019a; Cai et al., 2024). The ultra-high resolution (> 100,000), fast polarity and reagent switching, and multi-pressure scheme of the MION-Orbitrap enable the measurement of the full distribution of precursor molecules and their progressively oxygenated reaction products in atmospheric environments (Rissanen et al., 2019; Cai et al., 2024; Shcherbinin et al., 2024).

Two key challenges remain. First, any ionization reagent is inherently selective, making complete capture of all molecular species unattainable. Continued development of reagents with broader coverage is therefore essential. Second, authentic monomeric OOM standards, particularly those featuring peroxy acid functionalities, are not commercially available. The absence of suitable OOM standards critically constrains both the study of their detection by CIMS and the development of robust and precise calibration methods (Alage et al., 2024). Because their ionization efficiencies remain unknown, quantitative interpretation of OOM concentrations in the atmosphere, and thus accurate model representation, remains severely limited. While the synthesis of OOM dimers has been demonstrated (Kenseth et al., 2020, 2023; Li et al., 2024), only a few studies have attempted OOM monomer synthesis, successfully producing α-pinene-derived monoperoxypinic acid (Steimer et al., 2018) and hydroxy hydroperoxides (Mettke et al., 2022).

In this study, we synthesized two OOM monomers derived from α-pinene ozonolysis with molecular formulas $C_9H_{14}O_4$ and $C_{10}H_{16}O_4$, referred to as peroxy norpinonic acid (PNPA) and peroxy pinonic acid (PPA), respectively (structures depicted in Fig. 1). They represent the corresponding peroxy acids of norpinonic acid (NPA; $C_9H_{14}O_3$) and pinonic acid (PA; $C_{10}H_{16}O_3$), which are major oxidation products of α-pinene (Wilson et al., 1972; Hatakeyama et al., 1989; Kavouras et al., 1999; Yu et al., 1999). Both standards contain four oxygen atoms and are therefore classified as moderately oxygenated molecules (MOMs). Their peroxy acid functionality makes them useful model compounds for probing the detection of peroxy-acid-containing α-pinene-derived oxidation products, including HOMs, but they should not be treated as quantitative proxies for the broader and more highly functionalized HOM population. We confirmed their structures via ^{1}H and ^{13}C NMR (nuclear magnetic resonance) spectroscopy and subsequently investigated their detection with a MION-Orbitrap operated with nitrate (NO_3^-) and uronium ($CH_5N_2O^+$) (Shcherbinin et al., 2025). The gas-phase ionization was also compared to heated electrospray ionization (H-ESI). We show that these two peroxy acids exhibit strong variability in instrument response across different ionization schemes, indicating that their abundance may be substantially underestimated in atmospheric studies. Whether comparable response behavior occurs for more highly oxygenated atmospheric peroxy acids remains to be established using additional authentic standards.

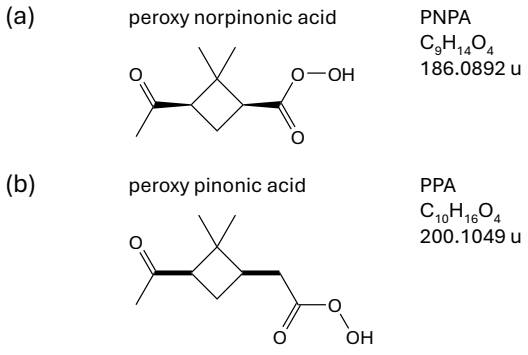

Figure 1. Synthesized oxygenated organic molecule (OOM) monomers: (a) peroxy norpinonic acid (PNPA; $C_9H_{14}O_4$; exact mass 186.0892 u) and (b) peroxy pinonic acid (PPA; $C_{10}H_{16}O_4$; exact mass 200.1049 u).

2 Materials and methods

2.1 Synthesized OOM standards

Figure 1 presents the molecular structures of our synthesized OOM monomers along with their full names, abbreviations, chemical formulas, and exact masses. Peroxy norpinonic acid (PNPA; $C_9H_{14}O_4$) and peroxy pinonic acid (PPA; $C_{10}H_{16}O_4$) exhibit exact masses of 186.0892 u and 200.1049 u, respectively. They were synthesized according to the procedure outlined in Appendix A, measured with ^{1}H and ^{13}C NMR (Bruker AC 400 MHz NMR spectrometer), and immediately prepared for and transferred to the mass spectrometric experimental setup.

2.2 Laboratory experiment

Figure 2 schematically illustrates the experimental setup comprising two pathways. In pathway (a), the synthesized standards were dissolved in deuterated chloroform (sample concentration: $\sim 75\,\mathrm{mg\,mL^{-1}}$) and introduced into an evaporator (solution volume: 0.6 mL), which was temperature-regulated to 20 °C by water circulating through its double wall from a thermal bath (Thermo Fisher Scientific Inc., Fisherbrand Isotemp 4100 R20F). A continuous stream of $2\,\mathrm{L\,min^{-1}}$ clean and dry compressed air was directed over the sample. The resulting vapor was diluted with $18\,\mathrm{L\,min^{-1}}$ of air in a sheath-flow configuration and transferred into the MION2 (Karsa Oy), where alternating gas-phase chemical ionization with nitrate (NO_3^-) and uronium ($CH_5N_2O^+$) reagent ions at atmospheric pressure was performed. Analyte ions were subsequently measured using an Orbitrap Exploris MX mass spectrometer (Thermo Fisher Scientific Inc.) with a mass resolution of 180,000 (at m/z 200). The sample lines were kept as short as practicable. A 70 mm long, 6 mm diameter PTFE tube connected the evaporator to a 260 mm long, 6 mm diameter stainless steel transfer tube. This tube was centered within the front side of the downstream stainless steel sheath-flow inlet assembly, which was 240 mm long and 24 mm in diameter. In pathway (b), the synthesized standards

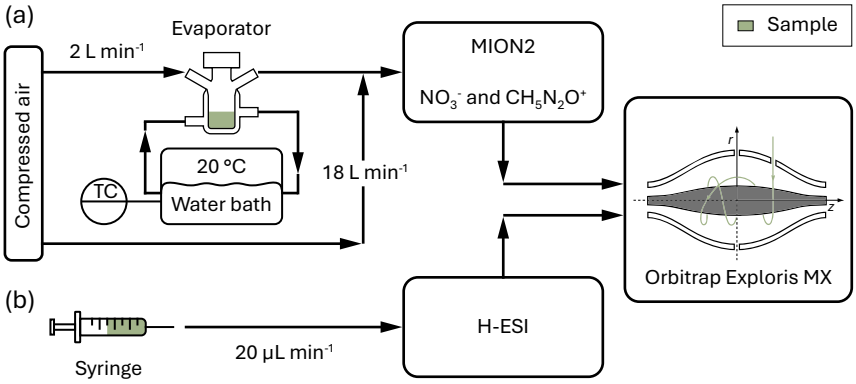

Figure 2. Laboratory experimental setup illustrating two independent approaches: (a) sample evaporation and gas-phase chemical ionization at atmospheric pressure using the multischeme chemical ionization inlet (MION2), and (b) liquid sample introduction and heated electrospray ionization (H-ESI). Orbitrap mass analyzer schematic adapted with permission from Thermo Fisher Scientific Inc. Abbreviations: TC: temperature controller; NO_3^-: nitrate; $CH_5N_2O^+$: uronium.

were dissolved in acetonitrile (sample concentration: $5 \times 10^{-3}\,\mathrm{mg\,mL^{-1}}$), filtered, and drawn into a syringe (solution volume: 0.4 mL). The sample solution was delivered at a flow rate of 20 $\mu\mathrm{L\,min^{-1}}$ through the capillaries into the H-ESI source, where ionization occurred prior to introduction into the Orbitrap.

The Orbitrap mass spectrometer was operated in negative polarity for nitrate and H-ESI measurements, and in positive polarity for uronium measurements, with a full scan range of 50–750 m/z, the RF Lens set to 70 %, standard AGC Target settings, and a maximum injection time of 100 ms. For MION2, the ion transfer tube temperature was set to 100 °C, whereas for H-ESI it was set to 320 °C. For H-ESI, the vaporizer temperature was 75 °C and the ion spray voltage was 2300 V. Mass calibration was performed using the Pierce FlexMix Calibration Solution (Thermo Fisher Scientific Inc.). Inter- and intra-sample variability were evaluated by repeating the synthesis and experimental procedures multiple times. PNPA was synthesized three times, yielding a total of six experimental repetitions. PPA was synthesized once and analyzed across three experimental repetitions. The experiments were also repeated with pure pinonic acid (PA) and commercial *meta*-Chloroperoxybenzoic acid (*m*CPBA ($C_7H_5ClO_3$); $\leq 77\,\%$ assay; remainder predominantly *meta*-Chlorobenzoic acid (*m*CBA) ($C_7H_5ClO_2$) and water), each conducted three times. Between experiments, the evaporator, connecting tubing, and inlet components up to the ion transfer tube were cleaned with acetone.

2.3 Data analysis

Mass spectra were acquired using Tune (Thermo Fisher Scientific Inc.). Four-minute averaged spectra were exported via FreeStyle (Thermo Fisher Scientific Inc.), and mass peaks of interest were extracted and normalized to primary ions for nitrate and uronium, and to the total ion count (TIC) for H-ESI. In MION2, ionization occurred predominantly through (de)protonation

Table 1. Ionization methods, associated ion species of interest, and exact masses for ions generated from the synthesized molecules (PNPA ($C_9H_{14}O_4$), PPA ($C_{10}H_{16}O_4$)) and their corresponding carboxylic acids (NPA ($C_9H_{14}O_3$), PA ($C_{10}H_{16}O_3$)).

Ionization method	Ion species	Molecules and exact ion masses (u)			
		$C_9H_{14}O_4$	$C_9H_{14}O_3$	$C_{10}H_{16}O_4$	$C_{10}H_{16}O_3$
MION2 (nitrate) & H-ESI	$[M - H]^-$	185.0814	169.0865	199.0970	183.1021
MION2 (uronium)	$[M + H]^+$	187.0970	171.1021	201.1127	185.1178
MION2 (nitrate)	$[M + NO_3]^-$	248.0770	232.0821	262.0927	246.0978
MION2 (uronium)	$[M + CH_5N_2O]^+$	247.1294	231.1345	261.1450	245.1501

and adduct formation, whereas H-ESI primarily achieved analyte ionization via deprotonation. Table 1 summarizes the masses of interest for each ionization method and OOM standard, including those corresponding to the carboxylic acids norpinonic acid (NPA; $C_9H_{14}O_3$) and pinonic acid (PA; $C_{10}H_{16}O_3$). All analyte peaks were considered detected only when their signal exceeded the corresponding blank mean by three standard deviations (3σ).

3 Results and discussion

Due to the synthesis procedure, each sample of synthesized standards contained a specific ratio of peroxy acids to their corresponding carboxylic acids. Figure 3 displays these ratios for both OOM standards measured by NMR and Orbitrap immediately after synthesis, as described in the previous section. Orbitrap ratios were computed from normalized peak intensities and averaged across repeated experiments; the plotted values represent the mean and the standard uncertainty derived from all measurements. NMR yielded the highest ratios (4.4 for PNPA and 4.7 for PPA), indicating that the freshly prepared standards were dominated by peroxy acids. In contrast, Orbitrap measurements produced significantly lower ratios. The only cases approaching or exceeding unity were nitrate adduct ionization for PNPA (0.87 ± 0.22; consistent with unity within uncertainty) and uronium adduct ionization for PPA (1.77), both indicating a higher abundance of peroxy acids than carboxylic acids, yet still yielding ratios substantially lower than those determined by NMR. Deprotonation and protonation yielded considerably lower ratios (0.03 to 0.39). These discrepancies reflect fundamental differences between techniques: NMR reports bulk composition in a fully non-perturbative, sample-preserving manner, whereas mass spectrometry reports only the fraction of molecules that successfully transfer, ionize, and survive to detection – processes that are inherently sensitive to evaporation and ionization efficiency, in-source chemistry, and matrix effects such as ion suppression. Consequently, the measured mass spectrometric signal response represents an interplay between (i) evaporation and transport kinetics from the liquid sample solution into the gas phase and onward to the Orbitrap, (ii) intrinsic molecular properties such as carbon number, functional group arrangement, and O – O bond lability, and (iii) the ionization pathway, including its efficiency, softness or hardness (adduct formation vs. (de)protonation), clustering energetics, and reagent selectivity.

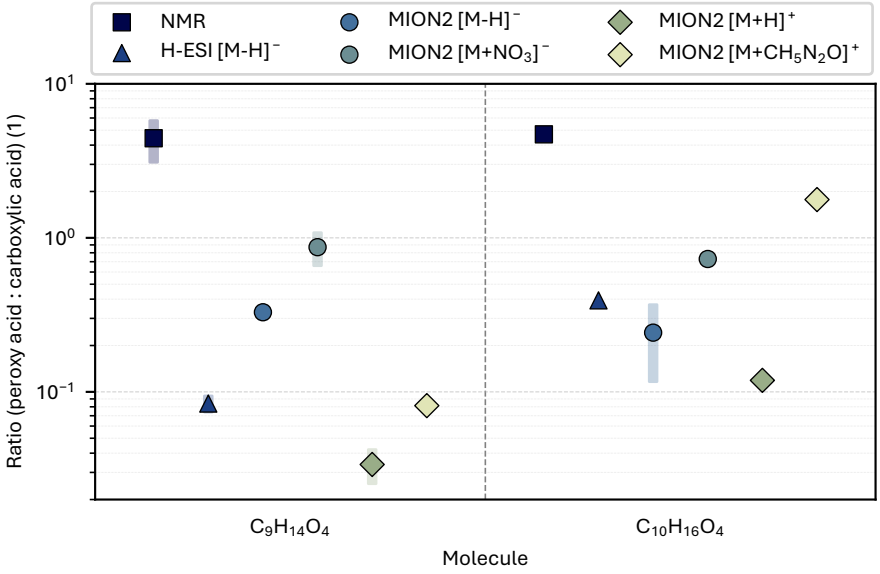

Figure 3. Ratios of peroxy acids to their corresponding carboxylic acids for PNPA ($C_9H_{14}O_4$) and PPA ($C_{10}H_{16}O_4$) measured by NMR and MION- and H-ESI-Orbitrap. Symbols represent mean ratios, and shaded areas indicate standard uncertainties calculated from all repeated syntheses and measurements. If no error bar is visible, it is obscured by the symbol. Circles represent MION-Orbitrap operated with nitrate, and diamonds represent MION-Orbitrap operated with uronium.

This framework also clarifies the role of our gas-phase experimental approach (pathway (a) in Fig. 2), which relies on evaporation of the liquid sample in the evaporator followed by transport of the volatilized molecules in an airstream toward the MION-Orbitrap. Under these conditions, any observed ratio between peroxy acids and carboxylic acids may be influenced by differences in their inherent volatilities. Table 2 lists the saturation mass concentrations and liquid vapor pressures of the synthesized OOM standards, *m*CPBA, and their corresponding carboxylic acids, calculated using the SIMPOL.1 group contribution method (Pankow and Asher, 2008). Their saturation mass concentrations, which are on the order of 10^2 to 10^5 $\mu g\,m^{-3}$, classify these molecules as intermediate volatility organic compounds (IVOCs) (Donahue et al., 2009; Stolzenburg et al., 2022).

These calculations predict that, at 20 °C, peroxy acids exhibit higher liquid vapor pressures and saturation concentrations, and therefore greater volatility, than the corresponding carboxylic acids (Table 2). Under these conditions, we would therefore expect preferential evaporation and more efficient transfer of peroxy acids into the gas stream and to the MION2, resulting in an even higher ratio of peroxy to carboxylic acids reaching MION2, being ionized, and ultimately detected in the Orbitrap than measured by NMR.

Figure 4 shows a representative time trace of the nitrate adduct signals for *m*CPBA and *m*CBA, along with the temporal evolution of the peroxy-to-carboxylic-acid ratio. The initial ~ 25 min correspond to blank measurements, while the pronounced increase in signal intensity at ~ 30 min indicates the start of sample evaporation following introduction into the evaporator. Consistent with the SIMPOL.1 group contribution predictions at 20 °C, where the peroxy acid functional group yields a higher

Table 2. Saturation mass concentrations $\log_{10}(c^{\circ})$ and liquid vapor pressures p_{L}° for the synthesized molecules (PNPA ($C_9H_{14}O_4$), PPA ($C_{10}H_{16}O_4$)), *meta*-Chloroperoxybenzoic acid (*m*CPBA; $C_7H_5ClO_3$), and their corresponding carboxylic acids (NPA ($C_9H_{14}O_3$), PA ($C_{10}H_{16}O_3$), and *meta*-Chlorobenzoic acid (*m*CBA; $C_7H_5ClO_2$)), calculated using the SIMPOL.1 group contribution method (Pankow and Asher, 2008).

Molecule	Saturation mass concentration $\log_{10}(c^{\circ}[\mu\mathrm{g\,m^{-3}}])$	Vapor pressure p_{L}° (Pa)
$C_9H_{14}O_4$	4.32	2.72×10^{-1}
$C_9H_{14}O_3$	3.18	2.16×10^{-2}
$C_{10}H_{16}O_4$	3.91	9.94×10^{-2}
$C_{10}H_{16}O_3$	2.78	7.90×10^{-3}
$C_7H_5ClO_3$	5.43	3.81×10^{0}
$C_7H_5ClO_2$	4.29	3.03×10^{-1}

vapor pressure and therefore a higher saturation concentration than the corresponding carboxylic acid group, the *m*CPBA control experiment exhibits the expected volatility contrast: *m*CPBA produces a strong, early-rising nitrate adduct signal, whereas the *m*CBA signal appears more slowly and at substantially lower intensity. This difference in evaporation kinetics is reflected in the peroxy-to-carboxylic-acid ratio, which increases gradually over $\sim 12\,\mathrm{min}$ before approaching a steady plateau, indicating the time required for the less volatile *m*CBA to accumulate in the gas phase. The peroxy acid signal is roughly two orders of magnitude higher than that of the carboxylic acid, consistent with both its greater volatility and its larger fraction in the technical *m*CPBA mixture. Together, these observations reflect the behavior predicted by SIMPOL.1 and demonstrate the characteristic signature of two species with distinctly different volatilities evaporating independently and being transferred to the MION2 and ultimately detected in the Orbitrap.

Figure 5 shows representative time traces for the nitrate and uronium adduct signals of PNPA/NPA and PPA/PA, respectively, together with the time evolution of the peroxy-to-carboxylic-acid ratio. The first $\sim 25\,\mathrm{min}$ capture blank measurements in both ionization modes. The persistent signals at mass-to-charge ratios (m/z) 247 and 231 during the initial uronium blank are attributed to trace carryover retained on inlet or instrument surfaces and detected because of the high sensitivity of uronium; all reported sample signals nevertheless exceeded the corresponding blank-derived 3σ threshold. The onset of sample introduction into the evaporator and subsequent evaporation is evident from the sharp intensity increases in uronium mode at $\sim 27\,\mathrm{min}$ in Fig. 5a and $\sim 30\,\mathrm{min}$ in Fig. 5b. The nitrate adduct signal is already stabilized when that mode is engaged. In contrast to both the SIMPOL.1 predictions and the behavior observed for the *m*CPBA control, both synthesized OOM standards exhibit a distinctly different pattern: the peroxy acid and carboxylic acid signals rise simultaneously after sample introduction and follow nearly identical temporal profiles. This is reflected directly in the peroxy-to-carboxylic-acid ratio, which, after a brief stabilization period during the onset of evaporation, remains constant over time and reaches this steady level within only 1 to $2\,\mathrm{min}$. Moreover, the signal intensities deviate strongly from expectations based on NMR measurements and SIMPOL-derived

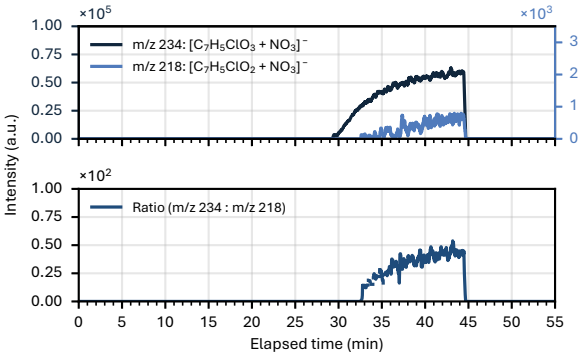

Figure 4. Extracted-ion chromatogram of the nitrate adduct ions of *meta*-Chloroperoxybenzoic acid (*m*CPBA; $C_7H_5ClO_3$; m/z 234 for the nitrate adduct) and *meta*-Chlorobenzoic acid (*m*CBA; $C_7H_5ClO_2$; m/z 218 for the nitrate adduct). Absolute intensities and the ratio (peroxy acid to carboxylic acid) are shown.

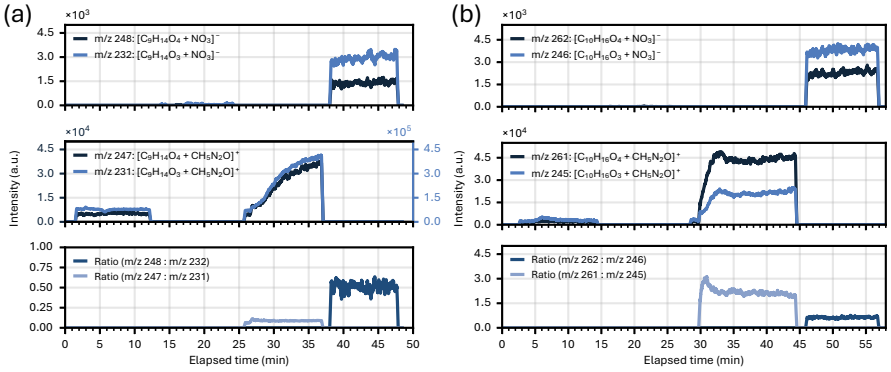

Figure 5. Extracted-ion chromatograms of the nitrate and uronium adduct ions of (a) peroxy norpinonic acid (PNPA; $C_9H_{14}O_4$; m/z 248 for the nitrate adduct and 247 for the uronium adduct) and norpinonic acid (NPA; $C_9H_{14}O_3$; m/z 232 for the nitrate adduct and 231 for the uronium adduct) and (b) peroxy pinonic acid (PPA; $C_{10}H_{16}O_4$; m/z 262 for the nitrate adduct and 261 for the uronium adduct) and pinonic acid (PA; $C_{10}H_{16}O_3$; m/z 246 for the nitrate adduct and 245 for the uronium adduct). Absolute intensities and the ratios (peroxy acid to carboxylic acid) are shown.

volatility differences: instead of the peroxy acids dominating and producing ratios higher than those measured by NMR, the carboxylic acid signals exceed the peroxy acid signals in most cases, with all measured ratios indicating a relative enrichment of carboxylic acids compared to the NMR values. Taken together, these observations support a consistent interpretation: the same parent species (predominantly the peroxy acids) evaporate into the gas phase, but a substantial fraction undergoes de-
175 composition, yielding two detectable signals – one corresponding to the surviving peroxy acids and the other to the carboxylic acids formed upon decomposition.

Decomposition of peroxy acids could in principle occur during transport, ionization, or another step prior to detection. However, several lines of evidence indicate that structural degradation most likely occurs during ionization. The O – O bond in the peroxy acid group is relatively weak and susceptible to cleavage. In liquid-phase electrospray (H-ESI), high electric fields (Gabelica and Pauw, 2005) and electrochemical processes at the emitter (Pozniak and Cole, 2015) can promote such bond rupture, particularly during (de)protonation pathways that impart considerable internal energy. Similarly, in gas-phase chemical ionization (MION2), proton-transfer reactions during collisions with reagent ions can destabilize the O – O bond, and electrostatic stress in the inlet may amplify this effect. By contrast, reagent ion adduct formation ionization (e.g., nitrate or uronium) is softer, relying on non-covalent clustering rather than covalent activation, and therefore better preserves fragile functionalities such as peroxy acid groups. This interpretation is consistent with the measured peroxy-to-carboxylic-acid ratios (Fig. 3), which show strong differences across ionization techniques (H-ESI vs. MION2), reagent ions (nitrate vs. uronium), and ionization mechanisms ((de)protonation vs. adduct formation), with higher ratios for adduct peaks compared to (de)protonated peaks. These systematic differences across ionization modes support the interpretation that decomposition occurs during ionization, rather than elsewhere in the mass spectrometer; if fragmentation were occurring inside the instrument, the peroxy-to-carboxylic-acid ratios would not depend so sensitively on the ionization pathway. This interpretation is further reinforced by the operating conditions of the Orbitrap Exploris MX: during full-MS^1 acquisition, MS/MS fragmentation is not engaged, and ions are transmitted to the mass analyzer without deliberate collisional activation, making decomposition in the instrument unlikely. Furthermore, our observations align with earlier findings by Steimer et al. (2018), who reported rapid decay of synthesized monoperoxypinic acid on filters – about 60 % lost within 5 h and measurable changes also in liquid samples over 22 h, underscoring the intrinsic instability of peroxy acids related to atmospheric BVOC autoxidation.

Taken together, only the *m*CPBA control reflects the SIMPOL.1 volatility expectation that peroxy acids evaporate more readily than their corresponding carboxylic acids, leading to a significantly greater fraction of peroxy acids orbiting around the mass analyzer and, consequently, a much higher detected signal. This can plausibly be attributed to aromatic stabilization from the benzene ring, which renders *m*CPBA more persistent than typical aliphatic peroxy acids.

A pure pinonic acid (PA) control experiment showed a markedly different temporal response from the PA signal in the PPA standard (Fig. S1). Pure PA continued to increase throughout the approximately 25 min uronium interval and retained a slightly increasing trend during the subsequent approximately 20 min nitrate interval, suggesting retention of the less volatile PA during evaporation and transport. In contrast, the PPA and PA signals in Fig. 5b rose rapidly together and approached a plateau within approximately 4 min. Because pure PA was measured using the same experimental setup and conditions, this difference argues against the PA signal in the synthesized sample arising predominantly from independently evaporating PA already present in the mixture. Although mixture composition may influence absolute evaporation rates, it does not readily explain the rapid, nearly identical profiles of the PPA and PA channels or the absence of the PA signal retention observed in the pure PA experiment. If the reduced PPA/PA ratio resulted primarily from a stronger compound-specific response to PA, the PA signal would still be expected to show the slower temporal response of independently evaporated PA. The comparison therefore argues against independent evaporation and compound-specific response factors as the main causes of the observed ratios and supports conversion from a common PPA-derived parent after evaporation and transport.

We further tested the influence of the ion transfer tube temperature. For the PPA standard measured in nitrate mode, increasing the temperature from 100 °C to 200 °C increased the PPA/PA nitrate adduct ratio from approximately 0.8 to approximately 1.0 (Fig. S2), which remained below the NMR ratio of 4.7. For commercial *m*CPBA measured with H-ESI, the deprotonated *m*CPBA/*m*CBA ratio increased from 0.02 at 85 °C to 0.03 at 110 °C and 0.04 at 320 °C (Fig. S3). In both experiments, higher transfer tube temperatures increased rather than decreased the relative peroxy acid signal. These results therefore exclude thermal degradation of peroxy acids in the ion transfer tube as a cause of the reduced ratios under the tested conditions.

Considering all experiments and controls, the systematically reduced peroxy-to-carboxylic-acid Orbitrap intensity ratios relative to NMR, the paired temporal profiles of the synthesized standards, and the strong dependence on ionization chemistry are consistent with ionization-associated loss of peroxy acid functionality. The pure PA control argues against independent evaporation of pre-existing PA and compound-specific response factors as the main explanations, and the temperature controls exclude thermal degradation in the ion transfer tube under the tested conditions. However, surface-catalyzed conversion at stainless steel inlet surfaces cannot be ruled out as a contributor to the reduced ratios.

Figure 6 compares intensities normalized to primary ions for nitrate and uronium adduct peaks of PNPA, PPA, and their corresponding carboxylic acids NPA and PA. The plotted values represent means with standard uncertainties from all measurements. Uronium adduct ionization consistently produced substantially higher intensities than nitrate adduct ionization, exceeding it by 1 to 2 orders of magnitude (factors ranging from 4×10^1 to 6×10^2). This trend is also reflected in the absolute intensities (see Fig. 5), indicating that the difference between the two ionization schemes is robust and not an artifact of normalization. Overall, these reagent-ion adduct intensity trends align well with chemical expectations. Nitrate is highly selective for HOMs and exhibits limited sensitivity to moderately oxygenated species (Riva et al., 2019b) such as PNPA, PPA, NPA, and PA. In contrast, uronium (protonated urea), a recently introduced positive-mode reagent, shows strong sensitivity for moderately oxygenated compounds (Shcherbinin et al., 2025), as evidenced by its consistently higher intensities than nitrate – also observable in blank measurements (Fig. 5) – confirming its suitability for this chemical space. On average, nitrate and uronium adduct signals for the peroxy acids were factors of 34 and 18 above their respective 3σ blank thresholds, indicating that both channels operated well beyond their detection limits and that their behavior was unlikely to be governed by near-limit effects.

As a limited validation of the nitrate response at low signal intensity, four *m*CPBA solution concentrations were measured. The deprotonated *m*CPBA signal was averaged over 9 min and normalized to the nitrate primary ions (Fig. S4). The response was described by $y = 1.213 \times 10^{-4} x + 6.440 \times 10^{-4}$ ($R^2 = 0.982$; $n = 4$). This result demonstrates a systematic concentration response for *m*CPBA within the relevant low-intensity regime. It does not determine the relative molar response factors of PNPA/NPA or PPA/PA; however, the pure PA temporal response shows that compound-specific response factors cannot account for the observed time profiles and are therefore unlikely to be the principal cause of the reduced ratios.

As seen in Fig. 3, the extent of peroxy acid loss depends on both the reagent-ion chemistry and the molecular structure of the analyte. Although uronium generally yields higher intensities than nitrate for both peroxy acids, it appears to induce greater in-source decomposition of PNPA while better preserving PPA; nonetheless, in both cases, the resulting peroxy-to-carboxylic-acid ratios remain substantially lower than expected from NMR and SIMPOL.1. This compound-specific behavior aligns with the

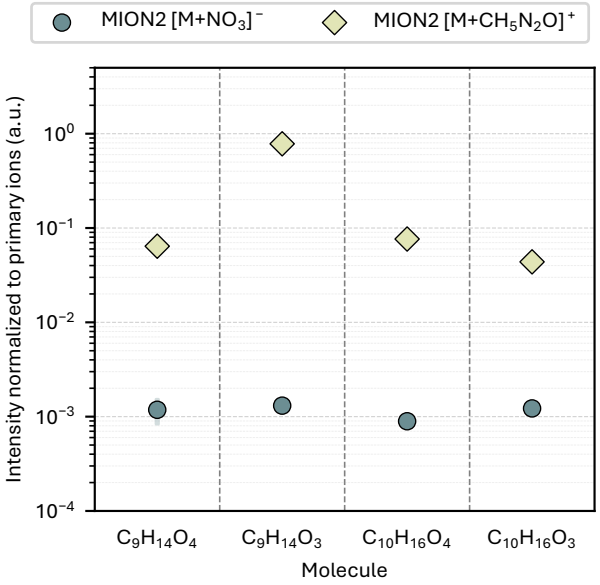

Figure 6. Intensities normalized to primary ions for nitrate and uronium adduct peaks of PNPA ($C_9H_{14}O_4$), PPA ($C_{10}H_{16}O_4$), and their corresponding carboxylic acids (NPA ($C_9H_{14}O_3$) and PA ($C_{10}H_{16}O_3$)). Symbols represent mean intensities, and shaded areas indicate standard uncertainties calculated from all repeated syntheses and measurements. If no error bar is visible, it is obscured by the symbol.

uronium-CI mechanism: Shcherbinin et al. (2025) show that uronium ionization is fundamentally controlled by analyte-specific cluster geometries, binding enthalpies, and stabilization efficiencies, implying intrinsically molecule-dependent sensitivities. Taken together, these observations add a final layer to our decomposition hypothesis: peroxy acid loss is dependent on both the ionization mechanism and the analyte.

4 Conclusions

In this work, we synthesized two monomeric OOM standards from α-pinene ozonolysis containing a peroxy acid functionality. With four oxygen atoms, they are moderately oxygenated molecules (MOMs). Because peroxy acid functionalities often occur in OOMs, including highly oxygenated organic molecules (HOMs), these standards can provide useful qualitative insight into their analytical behavior. However, they should not be regarded as quantitative proxies for the broader population of HOMs. We characterized their detectability with a nitrate- and uronium-based MION-Orbitrap and compared these two gas-phase ionization schemes with liquid H-ESI.

Across all techniques, NMR confirmed that the freshly synthesized standards were dominated by peroxy acids, whereas Orbitrap measurements consistently yielded substantially lower peroxy-to-carboxylic-acid ratios, contradicting the SIMPOL.1 expectation that the higher volatility of peroxy acids should produce ratios even greater than those measured by NMR. Crucially, the time evolution of these ratios supports peroxy acid decomposition: after a brief stabilization period, the peroxy-

to-carboxylic-acid ratios reach a constant level rapidly, and the peroxy and carboxylic acid signals exhibit nearly identical temporal profiles. In contrast, pure pinonic acid (PA), measured using the same experimental conditions, continued to increase over approximately 45 min and did not show the rapid plateau observed for the peroxy pinonic acid (PPA) standard, suggesting retention of the less volatile PA during evaporation and transport. This argues against independent evaporation and compound-specific response factors as the main causes of the reduced ratios and instead supports the interpretation that both signals originate from a common PPA-derived parent, with conversion occurring after evaporation. Increasing the ion transfer tube temperature did not decrease the relative peroxy acid response for either the PPA standard or *m*CPBA, excluding thermal degradation in the ion transfer tube under the tested conditions. Together with the divergence between sample-preserving NMR and sample-modifying mass spectrometric measurements, and with the pronounced variability across ionization modes, these observations are consistent with ionization-associated loss of peroxy-acid functionality. Such loss appears more pronounced under harder ionization pathways such as (de)protonation. Softer ionization routes such as nitrate and uronium adduct formation appear to preserve the peroxy acid functionality more effectively; nevertheless, even these channels yield ratios substantially below the bulk values, and the relative responses vary with reagent-ion chemistry and the molecular structure of the analyte, as indicated by the pronounced shifts in the peroxy-to-carboxylic-acid ratios for the two standards under uronium ionization. However, surface-catalyzed conversion at stainless steel inlet surfaces cannot be excluded as a possible contributor to the reduced ratios, highlighting the need for dedicated experiments assessing the influence of inlet material. Finally, our findings highlight that uronium adduct ionization captures this class of moderately oxygenated compounds far more efficiently than nitrate, underscoring its value as a complementary reagent for expanding molecular coverage beyond the HOM-biased selectivity of nitrate-CIMS.

Our results suggest that peroxy acids formed via autoxidation of α-pinene – and potentially other biogenic VOCs – may often be inaccurately quantified across commonly used mass spectrometric techniques. Because nitrate-CIMS is the most prevalent method for gas-phase HOM detection in new particle formation studies, analogous response biases could translate into substantial uncertainties when deriving atmospheric process rates, including nucleation and growth rates of freshly formed particles. For example, in volatility-basis-set derivations from atmospheric measurements, misidentifying peroxy acids as carboxylic acids would artificially lower their assigned oxygen number, thereby underestimating O:C ratios for OOMs and propagating systematic errors in inferred volatilities. The magnitude and broader atmospheric relevance of these effects cannot be inferred directly from the two moderately oxygenated standards studied here and will require investigation using additional authentic standards. These findings underscore the need for calibration procedures capable of capturing such compound-specific effects, together with continued exploration of novel reagent-ion chemistries that provide broader and more uniform coverage across the full range of molecular oxygenation states present in the atmosphere.

Data availability. The data underlying Figs. 3–6 and Supplementary Figs. S1–S4 are available at https://doi.org/10.48436/w7z9r-9x511.

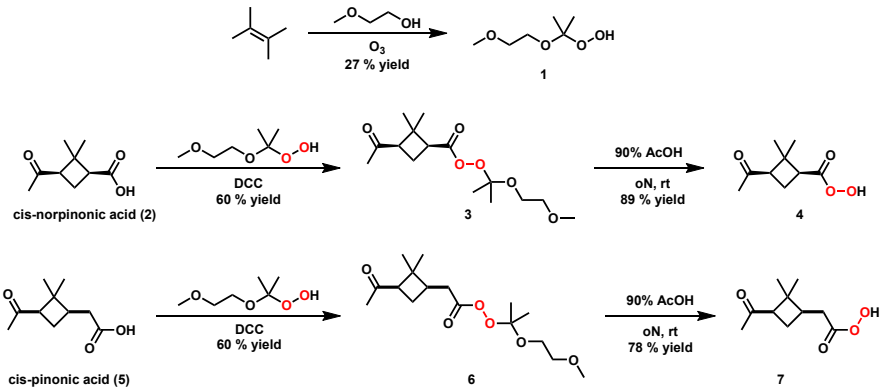

Figure A1. General scheme.

Appendix A: Synthesis

A1 General information

All reactions were stirred magnetically. Reagents were purchased from commercial suppliers and used as received. Dry dichloromethane (DCM) was retrieved from an Innovative Technologies PureSolv system. ^{1}H and ^{13}C NMR spectra were recorded on a Bruker AC 400 at 400 and 101 MHz; AC 600 at 600 and 151 MHz using the solvent peak as reference. The ratio of C9-peracid **4** and C9-acid **2** were determined by comparison of the signals at 2.77–2.67 ppm (m, 1H; for C9-peracid **4**) and 2.63–2.54 ppm (m, 1H; for C9-acid **2**). Multiplicities of ^{1}H signals were referred to as s (singlet), d (doublet), t (triplet), q (quartet) and more complex patterns or m (multiplet). ^{13}C NMR spectra were run in proton-decoupled mode. The ratio of C10-peracid **7** and C10-acid **5** were determined by comparison of the signals at 31.28 ppm (for C10-peracid **7**) and 34.65 ppm (for C10-acid **5**). TLC-analysis was done with precoated aluminum-backed plates (Silica gel 60 F254, Merck). Compounds were visualized by submerging in: an acidic phosphomolybdic acid / Cerium sulphate solution, $KMnO_4$, Vanillin or Anisaldehyde and dried with a heat gun. Column chromatography was carried out with silica gel Merck 60. Eluent systems refer to volumetric ratios, e.g., 4:1 = 80 % : 20 %. Specific rotations were measured on an Anton Parr MCP 500 polarimeter at 20 °C and 589 nm.

A2 General scheme

A3 2-Hydroperoxy-2-(2-methoxyethoxy)propane (1)

A 100 mL Schlenk flask charged with 2,3-dimethylbut-2-ene (1.98 mL, 16.63 mmol, 1 equiv.) in 40 ml methoxyethanol. Subsequently, 10 drops Sudan III indicator (0.01 M in DCM) were added and the pink solution was cooled to -80 °C. After 5 minutes, a stream of O_3 was passed through the reaction mixture until the pink color disappeared (approx. 8 minutes). Then,

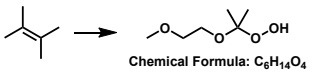

Figure A2. 2-Hydroperoxy-2-(2-methoxyethoxy)propane (**1**).

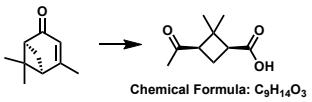

Figure A3. (1*S*,3*R*)-3-Acetyl-2,2-dimethylcyclobutane-1-carboxylic acid (***cis*-norpinonic acid (2)**).

a stream of O_2 was passed through for 5 minutes to remove excess O_3. The pale-yellow solution was directly subjected to distillation to remove the solvent. Subsequent high vacuum distillation furnished the desired product as colorless oil in 27 % yield (678 mg, 4.51 mmol).

b.p. 35 °C @ 0.75 mBar

Analytical data in accordance with literature: Dussault et al. (1994).

A4 (1*S*,3*R*)-3-Acetyl-2,2-dimethylcyclobutane-1-carboxylic acid (*cis*-norpinonic acid (2)

A flame-dried 100 mL Schlenk flask was charged with (*S*)-Verbenone [CAS 1196-01-6] (95 %, 2.0 g, 12.6 mmol, 1 equiv.) and dissolved in 20 mL dry acetonitrile. The colorless solution was cooled to -40 °C and a stream of O_3 was passed through the reaction mixture until the reaction mixture became yellow (approx. 30 minutes). Then, a stream of O_2 was passed through for 5 minutes to remove excess O_3. H_2O_2 (35 % in water, 11.1 mL, 126 mmol, 10 equiv.) was added and the mixture was allowed to warm to room temperature. The aqueous layer was extracted with $CHCl_3$ (8x), dried over $MgSO_4$ and concentrated in vacuo. The desired product was obtained as white solids in 99 % yield (2.13 g, 12.5 mmol).

^{1}H NMR (400 MHz, $CDCl_3$) δ 2.90 (dd, J = 10.7, 7.7 Hz, 1H), 2.82 (ddd, J = 9.4, 7.9, 1.4 Hz, 1H), 2.61 (dtd, J = 12.8, 10.8, 2.0 Hz, 1H), 2.07 (d, J = 1.1 Hz, 3H), 1.90 (ddd, J = 11.8, 8.9, 6.7 Hz, 1H), 1.45 (d, J = 1.4 Hz, 3H), 0.97 (d, J = 1.7 Hz, 3H).

^{13}C NMR (101 MHz, $CDCl_3$) δ 207.3, 178.2, 53.1, 45.1, 45.0, 30.3, 30.1, 18.9, 18.1.

$[\alpha]_D^{20}$ = -52.58 (c 1.60, CH_2Cl_2).

A5 2-(2-Methoxyethoxy)propan-2-yl (1*S*,3*R*)-3-acetyl-2,2-dimethylcyclobutane-1-carboperoxoat (3)

A 50 mL Schlenk flask was charged with ***cis*-norpinonic acid (2)** (1.27 g, 7.46 mmol, 1.2 equiv.) and *N,N*-dicyclohexylcarbodiimid (1.41 g, 6.84 mmol, 1.1 equiv.) in 30 mL dry DCM. To the white, turbid solution peroxide **1** (934 mg, 6.22 mmol, 1 equiv.) dissolved in 5 mL dry DCM was added, followed by 4-(dimethylamino)pyridine (76 mg, 0.62 mmol, 0.1 equiv.). The reaction was stirred at room temperature until TLC (petroleum ether/ethyl acetate 1:1, stained with anisaldehyde or vanillin stain) confirmed full conversion. Silica gel was added and all volatiles were removed in vacuo. The crude mixture was directly subjected

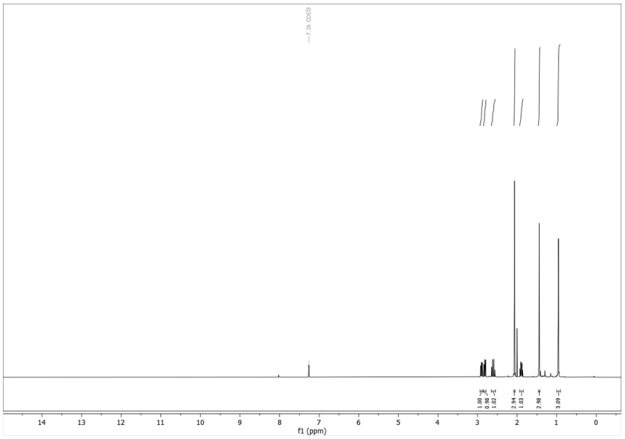

Figure A4. (1*S*,3*R*)-3-Acetyl-2,2-dimethylcyclobutane-1-carboxylic acid (***cis*-norpinonic acid (2)**). ^{1}H NMR (400 MHz, $CDCl_3$).

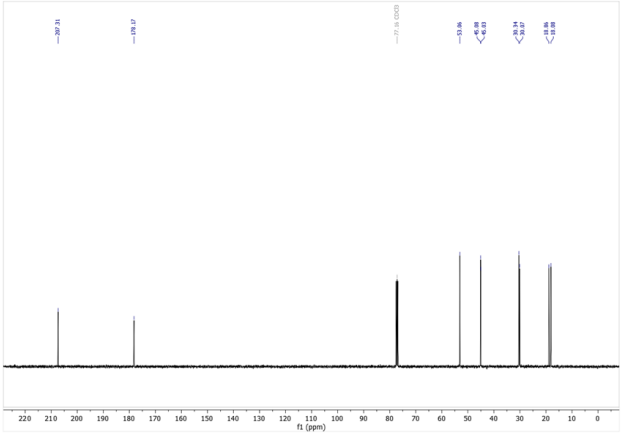

Figure A5. (1*S*,3*R*)-3-Acetyl-2,2-dimethylcyclobutane-1-carboxylic acid (***cis*-norpinonic acid (2)**). ^{13}C NMR (101 MHz, $CDCl_3$).

to column chromatography (190 g silica, petroleum ether/ethyl acetate 2:1) and the desired product was obtained as colorless oil in 60 % yield (1.13 g, 3.73 mmol).

^{1}H NMR (400 MHz, $CDCl_3$) δ 3.77–3.69 (m, 2H), 3.51–3.43 (m, 2H), 3.34 (s, 3H), 2.94–2.85 (m, 1H), 2.85–2.75 (m, 1H), 2.75–2.61 (m, 1H), 2.05 (s, 3H), 1.99–1.87 (m, 1H), 1.47 (s, 6H), 1.42 (s, 3H), 0.98 (s, 3H).

^{13}C NMR (101 MHz, $CDCl_3$) δ 206.5, 169.0, 106.9, 71.9, 61.6, 59.2, 53.3, 45.1, 42.7, 30.4, 30.0, 23.4, 23.1, 19.2, 18.4.

$[\alpha]_D^{20}$ = -18.26 (c 1.60, CH_2Cl_2).

HRMS (MION2-Orbitrap) $[M + CH_5N_2O]^+$ calculated 363.2131 u; found 363.2117 u.

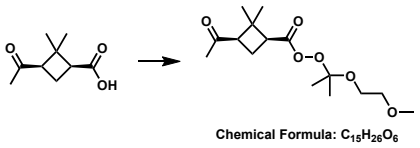

Figure A6. 2-(2-Methoxyethoxy)propan-2-yl (1*S*,3*R*)-3-acetyl-2,2-dimethylcyclobutane-1-carboperoxoat (**3**).

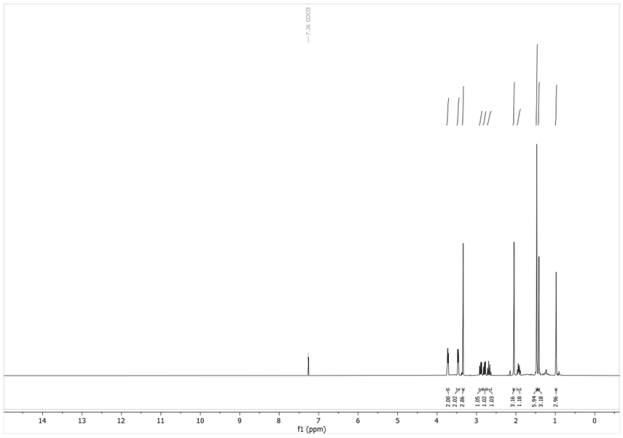

Figure A7. 2-(2-Methoxyethoxy)propan-2-yl (1*S*,3*R*)-3-acetyl-2,2-dimethylcyclobutane-1-carboperoxoat (**3**). ^{1}H NMR (400 MHz, $CDCl_3$).

A6 (1*S*,3*R*)-3-Acetyl-2,2-dimethylcyclobutane-1-carboperoxoic acid (4)

A 50 mL round bottom flask charged with perester **3** (269 mg, 0.89 mmol, 1 equiv.) in 4.46 mL (freshly prepared) 90 % acetic acid (60 mmol, 79 equiv.) and BHT (0.1M solution in Et_2O, 0.50 mL, 0.05 mmol, 0.06 equiv.). The clear colorless solution was stirred at room temperature for 24 hours, at which point TLC (petroleum ether/diethyl ether 1:3, stained with vanillin stain) confirmed full conversion. The reaction mixture was quenched by addition of saturated aqueous $NaHCO_3$ solution until pH=7 was reached (150 mL). The aqueous layer was extracted with Et_2O (4x 150 mL) and the combined organic layer was washed with small portions of saturated aqueous $NaHCO_3$ (2x 20 mL). It was dried over $MgSO_4$ and the solvent was removed in vacuo. The crude colorless oil was subjected to high vacuum which resulted in solidification of the material. The desired product was obtained as pale-yellow solids in 89 % yield (148 mg, 0.80 mmol) as a 7.1:1 mixture of peracid **4** : acid **2**.

^{1}H NMR (400 MHz, $CDCl_3$) δ 11.33 (d, J = 3.4 Hz, 1H), 2.96 (dd, J = 10.6, 7.7 Hz, 1H), 2.90 (dd, J = 10.7, 8.0 Hz, 1H), 2.80–2.71 (m, 1H), 2.08 (s, 3H), 2.03–1.95 (m, 1H), 1.45 (s, 3H), 0.96 (s, 3H).

^{13}C NMR (151 MHz, $CDCl_3$) δ 206.5, 172.6, 53.2, 45.2, 42.1, 30.3, 30.0, 18.8, 18.3.

$[\alpha]_D^{20}$ = -11.24 (c 1.70, CH_2Cl_2).

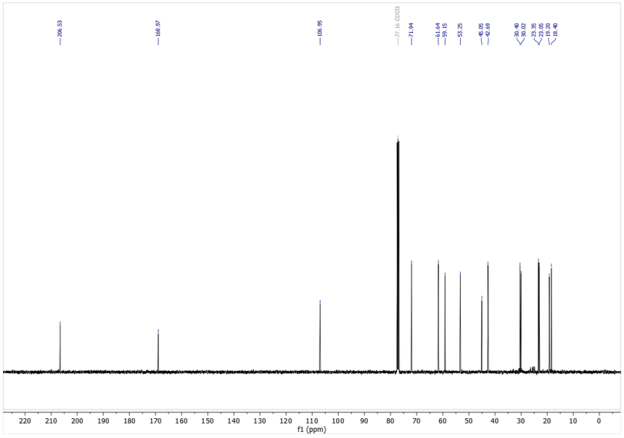

Figure A8. 2-(2-Methoxyethoxy)propan-2-yl (1*S*,3*R*)-3-acetyl-2,2-dimethylcyclobutane-1-carboperoxoat (**3**). ^{13}C NMR (101 MHz, $CDCl_3$).

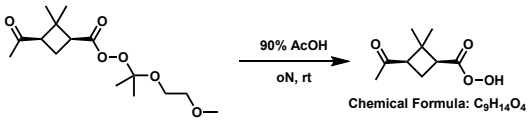

Figure A9. (1*S*,3*R*)-3-Acetyl-2,2-dimethylcyclobutane-1-carboperoxoic acid (**4**).

A7 *Cis*-2-(2-Methoxyethoxy)propan-2-yl 2-(3-acetyl-2,2-dimethylcyclobutyl)ethaneperoxoate (6)

A 50 mL Schlenk flask was charged with commercially available ***cis*-pinonic acid (5)** [CAS 61826-55-9] (763 mg, 4.14 mmol, 1.2 equiv.) and *N,N*-dicyclohexylcarbodiimid (783 mg, 3.80 mmol, 1.1 equiv.) in 15 mL dry DCM. To the white, turbid solution peroxide **1** (518 mg, 3.45 mmol, 1 equiv.) dissolved in 2.5 mL dry DCM was added, followed by 4-(dimethylamino)pyridine (42 mg, 0.35 mmol, 0.1 equiv.). The reaction was stirred at room temperature until TLC (petroleum ether/ethyl acetate 1:1, stained with anisaldehyde or vanillin stain) confirmed full conversion. Silica gel was added and all volatiles were removed in vacuo. The crude mixture was directly subjected to column chromatography (100 g silica, petroleum ether/ethyl acetate 2:1) and the desired product was obtained as white oily solids in 59 % yield (643 mg, 2.03 mmol).

^{1}H NMR (600 MHz, $CDCl_3$) δ 3.74–3.68 (m, 2H), 3.50–3.45 (m, 2H), 3.35 (s, 3H), 2.87 (dd, J = 10.2, 7.6 Hz, 1H), 2.40–2.29 (m, 2H), 2.24 (dd, J = 15.3, 7.6 Hz, 1H), 2.02 (s, 3H), 2.01–1.90 (m, 2H), 1.46 (s, 6H), 1.32 (s, 3H), 0.85 (s, 3H).

^{13}C NMR (151 MHz, $CDCl_3$) δ 207.3, 169.8, 107.0, 71.9, 61.6, 59.2, 54.2, 43.4, 38.0, 32.0, 30.3, 30.2, 23.1, 23.1, 23.1, 17.4.

HRMS (MION2-Orbitrap) $[M + CH_5N_2O]^+$ calculated 377.2288 u; found 377.2276 u.

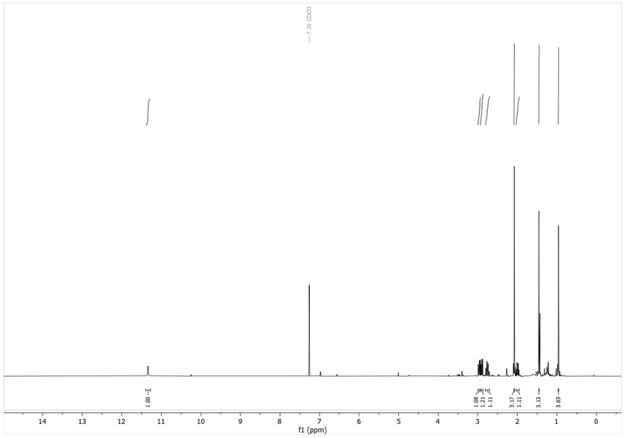

Figure A10. (1*S*,3*R*)-3-Acetyl-2,2-dimethylcyclobutane-1-carboperoxoic acid (**4**). ^{1}H NMR (400 MHz, $CDCl_3$).

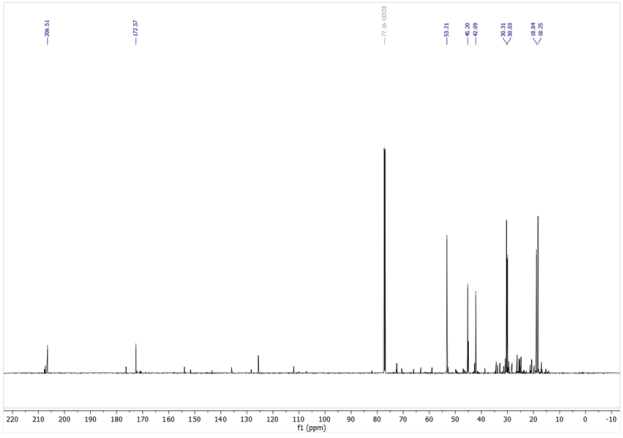

Figure A11. (1*S*,3*R*)-3-Acetyl-2,2-dimethylcyclobutane-1-carboperoxoic acid (**4**). ^{13}C NMR (151 MHz, $CDCl_3$).

A8 *Cis*-2-(3-Acetyl-2,2-dimethylcyclobutyl)ethaneperoxoic acid (7)

A 100 mL round bottom flask charged with perester **6** (509 mg, 1.61 mmol, 1 equiv.) in 5.4 mL (freshly prepared) 90 % acetic acid (85.3 mmol, 53 equiv.) and BHT (0.1M solution in Et_2O, 0.30 mL, 0.03 mmol, 0.02 equiv.). The clear colorless solution was stirred at room temperature for 18 hours, at which point TLC (DCM/MeOH 10:1, stained with vanillin stain) confirmed full conversion. The reaction mixture was quenched by addition of saturated aqueous $NaHCO_3$ solution until pH=7 was reached (300 mL). The aqueous layer was extracted with Et_2O (4x 250 mL) and the combined organic layer was washed with small portions of saturated aqueous $NaHCO_3$ (2x 50 mL). It was dried over $MgSO_4$ and the solvent was removed in vacuo. The crude colorless oil was subjected to high vacuum, and the desired product was obtained as colorless oil in 78 % yield (250 mg, 1.25 mmol) as 10.2:1 mixture of peracid **7** : acid **5**.

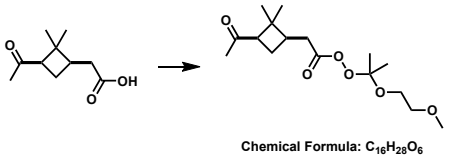

Figure A12. *Cis*-2-(2-Methoxyethoxy)propan-2-yl 2-(3-acetyl-2,2-dimethylcyclobutyl)ethaneperoxoate (**6**).

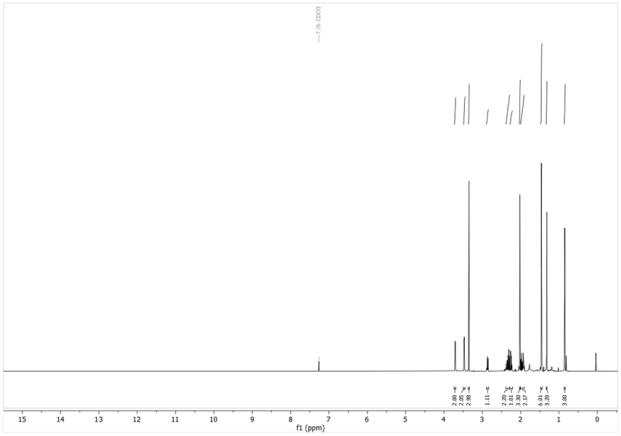

Figure A13. *Cis*-2-(2-Methoxyethoxy)propan-2-yl 2-(3-acetyl-2,2-dimethylcyclobutyl)ethaneperoxoate (**6**). ^{1}H NMR (600 MHz, $CDCl_3$).

^{1}H NMR: Peracid **7** not distinguishable from acid **5**.

^{13}C NMR (101 MHz, $CDCl_3$) δ 208.0, 172.6, 53.9, 43.3, 37.6, 31.3, 30.1, 30.0, 22.9, 17.2.

Author contributions. MT, RV, JB, DSc, ML, MO, and MK performed the experiments. MT analyzed the data. MT, MK, and DS wrote the manuscript. MT, MK, DS, PG, and HG were involved in supervision and in the interpretation of the scientific results. DS conceptualized the study. All authors commented on the manuscript.

Competing interests. The authors declare that they have no conflict of interest.

Acknowledgements. This research was funded by the Vienna Science and Technology Fund (WWTF, project VRG22-003) and the Austrian Science Fund (FWF, projects PAT8221324 and P35623-N).

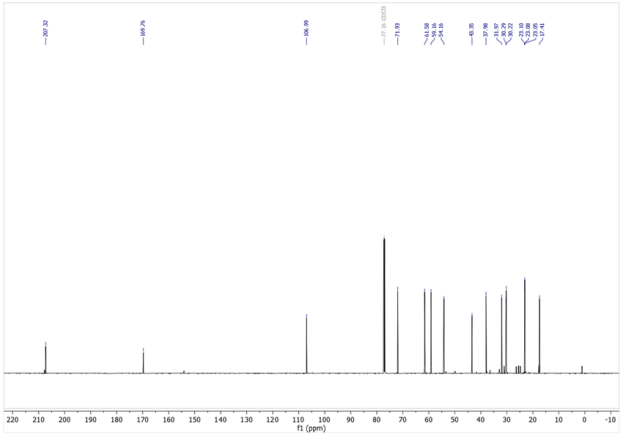

Figure A14. *Cis*-2-(2-Methoxyethoxy)propan-2-yl 2-(3-acetyl-2,2-dimethylcyclobutyl)ethaneperoxoate (**6**). ^{13}C NMR (151 MHz, $CDCl_3$).

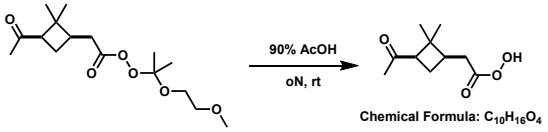

Figure A15. *Cis*-2-(3-Acetyl-2,2-dimethylcyclobutyl)ethaneperoxoic acid (**7**).

References

Alage, S., Michoud, V., Harb, S., Picquet-Varrault, B., Cirtog, M., Kumar, A., Rissanen, M., and Cantrell, C.: A nitrate ion chemical-ionization atmospheric-pressure-interface time-of-flight mass spectrometer (NO_3^- ToFCIMS) sensitivity study, Atmospheric Measurement Techniques, 17, 4709–4724, https://doi.org/10.5194/amt-17-4709-2024, 2024.

Bianchi, F., Kurtén, T., Riva, M., Mohr, C., Rissanen, M. P., Roldin, P., Berndt, T., Crounse, J. D., Wennberg, P. O., Mentel, T. F., Wildt, J., Junninen, H., Jokinen, T., Kulmala, M., Worsnop, D. R., Thornton, J. A., Donahue, N., Kjaergaard, H. G., and Ehn, M.: Highly Oxygenated Organic Molecules (HOM) from Gas-Phase Autoxidation Involving Peroxy Radicals: A Key Contributor to Atmospheric Aerosol, Chemical Reviews, 119, 3472–3509, https://doi.org/10.1021/acs.chemrev.8b00395, 2019.

Cai, C., Zhang, X., Wang, K., Zhang, Y., Wang, L., Zhang, Q., Duan, F., He, K., and Yu, S.-C.: Incorporation of new particle formation and early growth treatments into WRF/Chem: Model improvement, evaluation, and impacts of anthropogenic aerosols over East Asia, Atmospheric Environment, 124, 262–284, https://doi.org/10.1016/j.atmosenv.2015.05.046, 2016.

Cai, R., Mikkilä, J., Bengs, A., Koirala, M., Mikkilä, J., Holm, S., Juuti, P., Meder, M., Partovi, F., Shcherbinin, A., Worsnop, D., Ehn, M., and Kangasluoma, J.: Extending the Range of Detectable Trace Species with the Fast Polarity Switching of Chemical Ionization Orbitrap Mass Spectrometry, Analytical Chemistry, 96, 8604–8612, https://doi.org/10.1021/acs.analchem.4c00650, 2024.

Donahue, N. M., Robinson, A. L., and Pandis, S. N.: Atmospheric organic particulate matter: From smoke to secondary organic aerosol, Atmospheric Environment, 43, 94–106, https://doi.org/10.1016/j.atmosenv.2008.09.055, 2009.

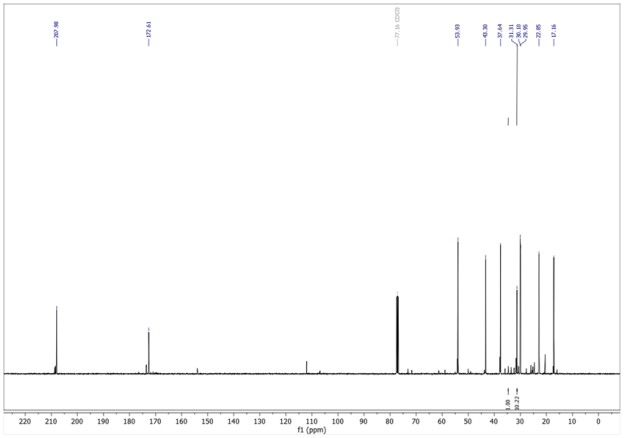

Figure A16. *Cis*-2-(3-Acetyl-2,2-dimethylcyclobutyl)ethaneperoxoic acid (**7**). ^{13}C NMR (101 MHz, $CDCl_3$).

Dussault, P. H., Zope, U. R., and Westermeyer, T. A.: 2-(2-Methoxyethoxy)prop-2-yl Hydroperoxide: An Easily Handled Reagent for the Synthesis of Alkyl Hydroperoxides, The Journal of Organic Chemistry, 59, 8267–8268, https://doi.org/10.1021/jo00105a053, 1994.

Ehn, M., Thornton, J. A., Kleist, E., Sipilä, M., Junninen, H., Pullinen, I., Springer, M., Rubach, F., Tillmann, R., Lee, B., Lopez-Hilfiker, F., Andres, S., Acir, I.-H., Rissanen, M., Jokinen, T., Schobesberger, S., Kangasluoma, J., Kontkanen, J., Nieminen, T., Kurtén, T., Nielsen, L. B., Jørgensen, S., Kjaergaard, H. G., Canagaratna, M., Maso, M. D., Berndt, T., Petäjä, T., Wahner, A., Kerminen, V.-M., Kulmala, M., Worsnop, D. R., Wildt, J., and Mentel, T. F.: A large source of low-volatility secondary organic aerosol, Nature, 506, 476–479, https://doi.org/10.1038/nature13032, 2014.

Elm, J., Myllys, N., and Kurtén, T.: What Is Required for Highly Oxidized Molecules To Form Clusters with Sulfuric Acid?, The Journal of Physical Chemistry A, 121, 4578–4587, https://doi.org/10.1021/acs.jpca.7b03759, 2017.

Fountoukis, C., Riipinen, I., Denier van der Gon, H. a. C., Charalampidis, P. E., Pilinis, C., Wiedensohler, A., O'Dowd, C., Putaud, J. P., Moerman, M., and Pandis, S. N.: Simulating ultrafine particle formation in Europe using a regional CTM: contribution of primary emissions versus secondary formation to aerosol number concentrations, Atmospheric Chemistry and Physics, 12, 8663–8677, https://doi.org/10.5194/acp-12-8663-2012, 2012.

Gabelica, V. and Pauw, E. D.: Internal energy and fragmentation of ions produced in electrospray sources, Mass Spectrometry Reviews, 24, 566–587, https://doi.org/10.1002/mas.20027, 2005.

Gordon, H., Kirkby, J., Baltensperger, U., Bianchi, F., Breitenlechner, M., Curtius, J., Dias, A., Dommen, J., Donahue, N. M., Dunne, E. M., Duplissy, J., Ehrhart, S., Flagan, R. C., Frege, C., Fuchs, C., Hansel, A., Hoyle, C. R., Kulmala, M., Kürten, A., Lehtipalo, K., Makhmutov, V., Molteni, U., Rissanen, M. P., Stozkhov, Y., Tröstl, J., Tsagkogeorgas, G., Wagner, R., Williamson, C., Wimmer, D., Winkler, P. M., Yan, C., and Carslaw, K. S.: Causes and importance of new particle formation in the present-day and preindustrial atmospheres, Journal of Geophysical Research: Atmospheres, 122, 8739–8760, https://doi.org/10.1002/2017JD026844, 2017.

Hallquist, M., Wenger, J. C., Baltensperger, U., Rudich, Y., Simpson, D., Claeys, M., Dommen, J., Donahue, N. M., George, C., Goldstein, A. H., Hamilton, J. F., Herrmann, H., Hoffmann, T., Iinuma, Y., Jang, M., Jenkin, M. E., Jimenez, J. L., Kiendler-Scharr, A., Maenhaut, W., McFiggans, G., Mentel, T. F., Monod, A., Prévôt, A. S. H., Seinfeld, J. H., Surratt, J. D., Szmigielski, R., and Wildt, J.: The formation,

properties and impact of secondary organic aerosol: current and emerging issues, Atmospheric Chemistry and Physics, 9, 5155–5236, https://doi.org/10.5194/acp-9-5155-2009, 2009.

Hatakeyama, S., Izumi, K., Fukuyama, T., and Akimoto, H.: Reactions of ozone with α-pinene and β-pinene in air: Yields of gaseous and particulate products, Journal of Geophysical Research: Atmospheres, 94, 13 013–13 024, https://doi.org/10.1029/JD094iD10p13013, 1989.

HEI: State of Global Air Report 2025, Health Effects Institute (HEI), Boston, MA, https://www.stateofglobalair.org/resources/report/state-global-air-report-2025, 2025.

Hodzic, A., Kasibhatla, P. S., Jo, D. S., Cappa, C. D., Jimenez, J. L., Madronich, S., and Park, R. J.: Rethinking the global secondary organic aerosol (SOA) budget: stronger production, faster removal, shorter lifetime, Atmospheric Chemistry and Physics, 16, 7917–7941, https://doi.org/10.5194/acp-16-7917-2016, 2016.

IHME: Global Burden of Disease 2023: Findings from the GBD 2023 study, Institute for Health Metrics and Evaluation (IHME), Seattle, WA, https://www.healthdata.org/research-analysis/library/global-burden-disease-2023-findings-gbd-2023-study, 2025.

IPCC: Climate Change 2021: The Physical Science Basis, Contribution of Working Group I to the Sixth Assessment Report of the Intergovernmental Panel on Climate Change [Masson-Delmotte, V., P. Zhai, A. Pirani, S.L. Connors, C. Péan, S. Berger, N. Caud, Y. Chen, L. Goldfarb, M.I. Gomis, M. Huang, K. Leitzell, E. Lonnoy, J.B.R.Matthews, T.K. Maycock, T. Waterfield, O. Yelekçi, R. Yu, and B. Zhou (eds.)], Cambridge University Press, Cambridge, United Kingdom and New York, NY, USA, 2391 pp, https://doi.org/10.1017/9781009157896, 2021.

Jimenez, J. L., Canagaratna, M. R., Donahue, N. M., Prevot, A. S. H., Zhang, Q., Kroll, J. H., DeCarlo, P. F., Allan, J. D., Coe, H., Ng, N. L., Aiken, A. C., Docherty, K. S., Ulbrich, I. M., Grieshop, A. P., Robinson, A. L., Duplissy, J., Smith, J. D., Wilson, K. R., Lanz, V. A., Hueglin, C., Sun, Y. L., Tian, J., Laaksonen, A., Raatikainen, T., Rautiainen, J., Vaattovaara, P., Ehn, M., Kulmala, M., Tomlinson, J. M., Collins, D. R., Cubison, M. J., E., Dunlea, J., Huffman, J. A., Onasch, T. B., Alfarra, M. R., Williams, P. I., Bower, K., Kondo, Y., Schneider, J., Drewnick, F., Borrmann, S., Weimer, S., Demerjian, K., Salcedo, D., Cottrell, L., Griffin, R., Takami, A., Miyoshi, T., Hatakeyama, S., Shimono, A., Sun, J. Y., Zhang, Y. M., Dzepina, K., Kimmel, J. R., Sueper, D., Jayne, J. T., Herndon, S. C., Trimborn, A. M., Williams, L. R., Wood, E. C., Middlebrook, A. M., Kolb, C. E., Baltensperger, U., and Worsnop, D. R.: Evolution of Organic Aerosols in the Atmosphere, Science, 326, 1525–1529, https://doi.org/10.1126/science.1180353, 2009.

Kavouras, I. G., Mihalopoulos, N., and Stephanou, E. G.: Formation and gas/particle partitioning of monoterpenes photo-oxidation products over forests, Geophysical Research Letters, 26, 55–58, https://doi.org/10.1029/1998GL900251, 1999.

Kenseth, C. M., Hafeman, N. J., Huang, Y., Dalleska, N. F., Stoltz, B. M., and Seinfeld, J. H.: Synthesis of Carboxylic Acid and Dimer Ester Surrogates to Constrain the Abundance and Distribution of Molecular Products in α-Pinene and β-Pinene Secondary Organic Aerosol, Environmental Science & Technology, 54, 12 829–12 839, https://doi.org/10.1021/acs.est.0c01566, 2020.

Kenseth, C. M., Hafeman, N. J., Rezgui, S. P., Chen, J., Huang, Y., Dalleska, N. F., Kjaergaard, H. G., Stoltz, B. M., Seinfeld, J. H., and Wennberg, P. O.: Particle-phase accretion forms dimer esters in pinene secondary organic aerosol, Science, 382, 787–792, https://doi.org/10.1126/science.adi0857, 2023.

Kirkby, J., Duplissy, J., Sengupta, K., Frege, C., Gordon, H., Williamson, C., Heinritzi, M., Simon, M., Yan, C., Almeida, J., Tröstl, J., Nieminen, T., Ortega, I. K., Wagner, R., Adamov, A., Amorim, A., Bernhammer, A.-K., Bianchi, F., Breitenlechner, M., Brilke, S., Chen, X., Craven, J., Dias, A., Ehrhart, S., Flagan, R. C., Franchin, A., Fuchs, C., Guida, R., Hakala, J., Hoyle, C. R., Jokinen, T., Junninen, H., Kangasluoma, J., Kim, J., Krapf, M., Kürten, A., Laaksonen, A., Lehtipalo, K., Makhmutov, V., Mathot, S., Molteni, U., Onnela, A., Peräkylä, O., Piel, F., Petäjä, T., Praplan, A. P., Pringle, K., Rap, A., Richards, N. A. D., Riipinen, I., Rissanen, M. P., Rondo, L., Sarnela,

N., Schobesberger, S., Scott, C. E., Seinfeld, J. H., Sipilä, M., Steiner, G., Stozhkov, Y., Stratmann, F., Tomé, A., Virtanen, A., Vogel, A. L., Wagner, A. C., Wagner, P. E., Weingartner, E., Wimmer, D., Winkler, P. M., Ye, P., Zhang, X., Hansel, A., Dommen, J., Donahue, N. M., Worsnop, D. R., Baltensperger, U., Kulmala, M., Carslaw, K. S., and Curtius, J.: Ion-induced nucleation of pure biogenic particles, Nature, 533, 521–526, https://doi.org/10.1038/nature17953, 2016.

Kulmala, M.: How Particles Nucleate and Grow, Science, 302, 1000–1001, https://doi.org/10.1126/science.1090848, 2003.

Kurtén, T., Rissanen, M. P., Mackeprang, K., Thornton, J. A., Hyttinen, N., Jørgensen, S., Ehn, M., and Kjaergaard, H. G.: Computational Study of Hydrogen Shifts and Ring-Opening Mechanisms in α-Pinene Ozonolysis Products, The Journal of Physical Chemistry A, 119, 11 366–11 375, https://doi.org/10.1021/acs.jpca.5b08948, 2015.

Li, K., Resch, J., and Kalberer, M.: Synthesis and Characterization of Organic Peroxides from Monoterpene-Derived Criegee Intermediates in Secondary Organic Aerosol, Environmental Science & Technology, 58, 3322–3331, https://doi.org/10.1021/acs.est.3c07048, 2024.

Lupascu, A., Easter, R., Zaveri, R., Shrivastava, M., Pekour, M., Tomlinson, J., Yang, Q., Matsui, H., Hodzic, A., Zhang, Q., and Fast, J. D.: Modeling particle nucleation and growth over northern California during the 2010 CARES campaign, Atmospheric Chemistry and Physics, 15, 12 283–12 313, https://doi.org/10.5194/acp-15-12283-2015, 2015.

Matsui, H., Koike, M., Takegawa, N., Kondo, Y., Takami, A., Takamura, T., Yoon, S., Kim, S.-W., Lim, H.-C., and Fast, J. D.: Spatial and temporal variations of new particle formation in East Asia using an NPF-explicit WRF-chem model: North-south contrast in new particle formation frequency, Journal of Geophysical Research: Atmospheres, 118, 11,647–11,663, https://doi.org/10.1002/jgrd.50821, 2013.

Mettke, P., Mutzel, A., Böge, O., Herrmann, H., Mettke, P., Mutzel, A., Böge, O., and Herrmann, H.: Synthesis and Characterization of Atmospherically Relevant Hydroxy Hydroperoxides, Atmosphere, 13, https://doi.org/10.3390/atmos13040507, 2022.

Pankow, J. F. and Asher, W. E.: SIMPOL.1: a simple group contribution method for predicting vapor pressures and enthalpies of vaporization of multifunctional organic compounds, Atmospheric Chemistry and Physics, 8, 2773–2796, https://doi.org/10.5194/acp-8-2773-2008, 2008.

Posner, L. N. and Pandis, S. N.: Sources of ultrafine particles in the Eastern United States, Atmospheric Environment, 111, 103–112, https://doi.org/10.1016/j.atmosenv.2015.03.033, 2015.

Pozniak, B. P. and Cole, R. B.: Perspective on Electrospray Ionization and Its Relation to Electrochemistry, Journal of the American Society for Mass Spectrometry, 26, 369–385, https://doi.org/10.1007/s13361-014-1066-x, 2015.

Qi, X., Ding, A., Roldin, P., Xu, Z., Zhou, P., Sarnela, N., Nie, W., Huang, X., Rusanen, A., Ehn, M., Rissanen, M. P., Petäjä, T., Kulmala, M., and Boy, M.: Modelling studies of HOMs and their contributions to new particle formation and growth: comparison of boreal forest in Finland and a polluted environment in China, Atmospheric Chemistry and Physics, 18, 11 779–11 791, https://doi.org/10.5194/acp-18-11779-2018, 2018.

Reddington, C. L., Carslaw, K. S., Spracklen, D. V., Frontoso, M. G., Collins, L., Merikanto, J., Minikin, A., Hamburger, T., Coe, H., Kulmala, M., Aalto, P., Flentje, H., Plass-Dülmer, C., Birmili, W., Wiedensohler, A., Wehner, B., Tuch, T., Sonntag, A., O'Dowd, C. D., Jennings, S. G., Dupuy, R., Baltensperger, U., Weingartner, E., Hansson, H.-C., Tunved, P., Laj, P., Sellegri, K., Boulon, J., Putaud, J.-P., Gruening, C., Swietlicki, E., Roldin, P., Henzing, J. S., Moerman, M., Mihalopoulos, N., Kouvarakis, G., Ždímal, V., Zíková, N., Marinoni, A., Bonasoni, P., and Duchi, R.: Primary versus secondary contributions to particle number concentrations in the European boundary layer, Atmospheric Chemistry and Physics, 11, 12 007–12 036, https://doi.org/10.5194/acp-11-12007-2011, 2011.

Rissanen, M. P., Mikkilä, J., Iyer, S., and Hakala, J.: Multi-scheme chemical ionization inlet (MION) for fast switching of reagent ion chemistry in atmospheric pressure chemical ionization mass spectrometry (CIMS) applications, Atmospheric Measurement Techniques, 12, 6635–6646, https://doi.org/10.5194/amt-12-6635-2019, 2019.

Riva, M., Ehn, M., Li, D., Tomaz, S., Bourgain, F., Perrier, S., and George, C.: CI-Orbitrap: An Analytical Instrument To Study Atmospheric Reactive Organic Species, Analytical Chemistry, 91, 9419–9423, https://doi.org/10.1021/acs.analchem.9b02093, 2019a.

Riva, M., Rantala, P., Krechmer, J. E., Peräkylä, O., Zhang, Y., Heikkinen, L., Garmash, O., Yan, C., Kulmala, M., Worsnop, D., and Ehn, M.: Evaluating the performance of five different chemical ionization techniques for detecting gaseous oxygenated organic species, Atmospheric Measurement Techniques, 12, 2403–2421, https://doi.org/10.5194/amt-12-2403-2019, 2019b.

Shcherbinin, A., Finkenzeller, H., Mikkilä, J., Kontro, J., Vinkvist, N., Kangasluoma, J., and Rissanen, M.: From Hydrocarbons to Highly Functionalized Molecules in a Single Measurement: Comprehensive Analysis of Complex Gas Mixtures by Multi-Pressure Chemical Ionization Mass Spectrometry, Analytical Chemistry, 96, 19 926–19 932, https://doi.org/10.1021/acs.analchem.4c03859, 2024.

Shcherbinin, A., Finkenzeller, H., Partovi, F., Vinkvist, N., Kontro, J., Boyer, M., Mikkilä, J., Iyer, S., Mikkilä, J., Juuti, P., Sarnela, N., Kangasluoma, J., and Rissanen, M.: Uronium from X-ray-Desorbed Urea Enables Sustainable Ultrasensitive Detection of Amines and Semivolatiles, Analytical Chemistry, 97, 21 282–21 290, https://doi.org/10.1021/acs.analchem.5c02239, 2025.

Sindelarova, K., Markova, J., Simpson, D., Huszar, P., Karlicky, J., Darras, S., and Granier, C.: High-resolution biogenic global emission inventory for the time period 2000–2019 for air quality modelling, Earth System Science Data, 14, 251–270, https://doi.org/10.5194/essd-14-251-2022, 2022.

Steimer, S. S., Delvaux, A., Campbell, S. J., Gallimore, P. J., Grice, P., Howe, D. J., Pitton, D., Claeys, M., Hoffmann, T., and Kalberer, M.: Synthesis and characterisation of peroxypinic acids as proxies for highly oxygenated molecules (HOMs) in secondary organic aerosol, Atmospheric Chemistry and Physics, 18, 10 973–10 983, https://doi.org/10.5194/acp-18-10973-2018, 2018.

Stolzenburg, D., Fischer, L., Vogel, A. L., Heinritzi, M., Schervish, M., Simon, M., Wagner, A. C., Dada, L., Ahonen, L. R., Amorim, A., Baccarini, A., Bauer, P. S., Baumgartner, B., Bergen, A., Bianchi, F., Breitenlechner, M., Brilke, S., Buenrostro Mazon, S., Chen, D., Dias, A., Draper, D. C., Duplissy, J., El Haddad, I., Finkenzeller, H., Frege, C., Fuchs, C., Garmash, O., Gordon, H., He, X., Helm, J., Hofbauer, V., Hoyle, C. R., Kim, C., Kirkby, J., Kontkanen, J., Kürten, A., Lampilahti, J., Lawler, M., Lehtipalo, K., Leiminger, M., Mai, H., Mathot, S., Mentler, B., Molteni, U., Nie, W., Nieminen, T., Nowak, J. B., Ojdanic, A., Onnela, A., Passananti, M., Petäjä, T., Quéléver, L. L. J., Rissanen, M. P., Sarnela, N., Schallhart, S., Tauber, C., Tomé, A., Wagner, R., Wang, M., Weitz, L., Wimmer, D., Xiao, M., Yan, C., Ye, P., Zha, Q., Baltensperger, U., Curtius, J., Dommen, J., Flagan, R. C., Kulmala, M., Smith, J. N., Worsnop, D. R., Hansel, A., Donahue, N. M., and Winkler, P. M.: Rapid growth of organic aerosol nanoparticles over a wide tropospheric temperature range, Proceedings of the National Academy of Sciences, 115, 9122–9127, https://doi.org/10.1073/pnas.1807604115, 2018.

Stolzenburg, D., Wang, M., Schervish, M., and Donahue, N. M.: Tutorial: Dynamic organic growth modeling with a volatility basis set, Journal of Aerosol Science, 166, 106 063, https://doi.org/10.1016/j.jaerosci.2022.106063, 2022.

Tröstl, J., Chuang, W. K., Gordon, H., Heinritzi, M., Yan, C., Molteni, U., Ahlm, L., Frege, C., Bianchi, F., Wagner, R., Simon, M., Lehtipalo, K., Williamson, C., Craven, J. S., Duplissy, J., Adamov, A., Almeida, J., Bernhammer, A.-K., Breitenlechner, M., Brilke, S., Dias, A., Ehrhart, S., Flagan, R. C., Franchin, A., Fuchs, C., Guida, R., Gysel, M., Hansel, A., Hoyle, C. R., Jokinen, T., Junninen, H., Kangasluoma, J., Keskinen, H., Kim, J., Krapf, M., Kürten, A., Laaksonen, A., Lawler, M., Leiminger, M., Mathot, S., Möhler, O., Nieminen, T., Onnela, A., Petäjä, T., Piel, F. M., Miettinen, P., Rissanen, M. P., Rondo, L., Sarnela, N., Schobesberger, S., Sengupta, K., Sipilä, M., Smith, J. N., Steiner, G., Tomè, A., Virtanen, A., Wagner, A. C., Weingartner, E., Wimmer, D., Winkler, P. M., Ye, P., Carslaw, K. S., Curtius, J., Dommen, J., Kirkby, J., Kulmala, M., Riipinen, I., Worsnop, D. R., Donahue, N. M., and Baltensperger, U.: The role of low-volatility organic compounds in initial particle growth in the atmosphere, Nature, 533, 527–531, https://doi.org/10.1038/nature18271, 2016.

Wilson, W. E., Schwartz, W. E., and Kinzer, G. W.: Haze formation: Its nature and origin, Tech. Rep. prepared for the Environmental Protection Agency (CPA 70-Neg. 172) and Coordinating Research Council (CAPA 6-68), Battelle Columbus Laboratories, 1972.

Yu, F. and Luo, G.: Simulation of particle size distribution with a global aerosol model: contribution of nucleation to aerosol and CCN number concentrations, Atmospheric Chemistry and Physics, 9, 7691–7710, https://doi.org/10.5194/acp-9-7691-2009, 2009.

Yu, J., Griffin, R. J., Cocker III, D. R., Flagan, R. C., Seinfeld, J. H., and Blanchard, P.: Observation of gaseous and particulate products of monoterpene oxidation in forest atmospheres, Geophysical Research Letters, 26, 1145–1148, https://doi.org/10.1029/1999GL900169, 1999.

Zhang, Q., Jimenez, J. L., Canagaratna, M. R., Allan, J. D., Coe, H., Ulbrich, I., Alfarra, M. R., Takami, A., Middlebrook, A. M., Sun, Y. L., Dzepina, K., Dunlea, E., Docherty, K., DeCarlo, P. F., Salcedo, D., Onasch, T., Jayne, J. T., Miyoshi, T., Shimono, A., Hatakeyama, S., Takegawa, N., Kondo, Y., Schneider, J., Drewnick, F., Borrmann, S., Weimer, S., Demerjian, K., Williams, P., Bower, K., Bahreini, R., Cottrell, L., Griffin, R. J., Rautiainen, J., Sun, J. Y., Zhang, Y. M., and Worsnop, D. R.: Ubiquity and dominance of oxygenated species in organic aerosols in anthropogenically-influenced Northern Hemisphere midlatitudes, Geophysical Research Letters, 34, https://doi.org/10.1029/2007GL029979, 2007.